Near Ultraviolet Emission Spectroscopy of the Hayabusa Re-entry

David Buttsworth*

University of Southern Queensland, Toowoomba, Queensland, Australia

Richard Morgan†

The University of Queensland, Brisbane, Queensland, Australia

Peter Jenniskens‡

SETI Institute, Mountain View, California

Quantitative time-resolved irradiance measurements were obtained of the Hayabusa Sample Return Capsule's entry on June 13, 2010, as measured from 12.6 km altitude with the Australian Ultraviolet Spectrograph instrument on board NASA's DC-8 Airborne Laboratory, which was stationed just outside of the landing site at the Woomera Test Range in Australia. The measurements were calibrated against NIST traceable standard calibration lamps on the tarmac at NASA Dryden Aircraft Operations Facility and at NASA Ames Research Center. The recorded spectra cover the wavelength range from 300 to 470 nm over the duration from 13:52:02.5 until 13:52:33.5 UTC. The spectra show shock emission from N_2^+, as well as several ablation products from the heat shield material (CN, Ca, and Al). In addition, the high-temperature tail of gray-body emission is observed to enter the wavelength range after 13:52:13 UTC. These data were evaluated in terms of the temporal evolution of the capsule's stagnation temperature and emissions within the CN and N_2^+ manifolds. A peak in the irradiance within the wavelength band from 365 to 392 nm was registered at approximately 13:52:07 UTC and elevated levels of irradiance within the combined

*Professor, Computational Engineering and Science Research Centre, University of Southern Queensland, 4350, Australia

†Professor, and Director, Centre for Hypersonics, The University of Queensland, 4072, Australia

‡Research Scientist, Carl Sagan Center, 189 Bernardo Avenue, Mountain View CA 94043, AIAA Member.

CN and N_2^+ manifolds were subsequently registered at about 13:52:20 UTC. An apparent maximum capsule temperature close to 3050 K was found at around 13:52:23 UTC, consistent with apparent capsule temperature values deduced using other instruments.

Nomenclature

A_i	aperture area of the instrument, m^2
A_l	lamp aperture area, m^2
A_{obs}	is instantaneous area of the capsule face observed from the DC-8, m^2
$E_{e,\lambda}$	spectral irradiance, W/m^2-nm
$L_{e,\lambda}$	spectral radiance, W/m^2-nm-sr
d_{obs}	instantaneous observed distance between the capsule and the DC-8, km
r_i	radius of the instrument aperture, m
r_{cap}	is the actual capsule radius, 0.2 m
x	is the distance from the source to the instrument aperture, m
Ω	solid angle

I. Introduction

Super-orbital re-entry still offers a host of challenges that are being tackled through the combined efforts of computational simulation and experimental measurements. To understand the minimum requirements of a thermal protection system's heat shield material, in-flight testing is ideal. However, current opportunities for flight testing of prototype configurations are rare and far between, so experimental efforts are generally focused on laboratory simulations.

In Australia, laboratory simulation of super-orbital flow energies is achieved using expansion tunnel facilities located at the University of Queensland.[1,2] These facilities are impulsive wind tunnel facilities which produce test flows with a duration on the order of 100 (and up to 500) microseconds. Actual flight conditions produce ablative flows for several tens of seconds under atmospheric conditions that are slightly different than in the wind tunnel facilities. Although recent free piston driver developments have established new flow conditions, scaled testing of thermal protection system models is commonly employed.

When an actual flight opportunity presented itself with the return of the JAXA Hayabusa Sample Return Capsule on the 13th of June 2010, the community worked together to mount an airborne and ground-based observing campaign to study the entry. Hayabusa was sched-

uled to enter the atmosphere above Australia late in the evening on the 13th of June 2010 with a speed of about 12.2 km/s, the fastest re-entry since 'Stardust' in 2006. Observations of the Stardust re-entry yielded a significant body of data suitable for testing computational models[3–5] so, with JAXA and Australian approval, NASA deployed the DC-8 Airborne Laboratory to the Woomera Test Range to provide a high altitude platform for Hayabusa irradiance measurements. A research team from the University of Southern Queensland and the University of Queensland contributed to this mission a near-UV slit-less spectrograph, called the Australian Ultraviolet Spectrograph (AUS). At the same time, teams of researchers from the University of Queensland, The University of Southern Queensland, and the University of New South Wales (Australian Defence Force Academy) were positioned at Tarcoola and Coober Pedy for ground-based observations of the re-entry.[6]

Near-UV emissions data were acquired using a variety of instruments during the Stardust re-entry observation campaign. The fibre-fed Cerny-Turner device described by Winter and Trumble[7] resolved CN and N_2^+ structures between about 320 and 450 nm with a resolution of about 0.3 nm for capsule altitudes between 75 and 50 km. Tracking challenges associated with the very narrow field of view of this device meant that not every recorded spectrum contained useful data. The echelle spectrograph used by Jenniskens[3] provided similar data but only at altitudes between 82 and 69 km whereas peak heating occurred at around 60 km. Lower resolution near-UV data was obtained for about 30 s around the time of peak heating using intensified video-rate devices down to wavelengths around 320 nm in the case of the work by Rairden and Jenniskens,[8] and down to about 380 nm in the case of the work by Jenniskens et al.[9] The $\Delta\nu = 0$ CN manifold was very well resolved by the upward-looking device of Jenniskens et al.[10] but only around the time of peak heating.

The AUS instrument was developed in an effort to provide near-UV emissions spectra from the Hayabusa re-entry to augment the existing Stardust data base. For the AUS instrument to make a useful contribution in this respect, it was determined that the CN and N_2^+ structures would need to be resolved, the deduced spectral emissions should have an absolute calibration reference, and reliable results were required throughout the re-entry process, including the time of peak heating.

Here, the results from the airborne observations of the Hayabusa re-entry obtained using the AUS device are discussed. Section II describes the AUS instrument and Section III details the calibration procedures and results. Section IV describes the data reduction techniques, presents the measured spectra, and discusses the temporal evolution of the irradiance signatures.

II. Instrument

The Australian Ultraviolet Spectrograph was mounted in the DC-8 at station 610 (the distance in inches from the nose of the aircraft). The instrument was co-aligned with an intensified near-UV spectrometer (IUV) as illustrated in Fig. 1. The IUV device was previously deployed in the Stardust observation campaign.[8] At station 610, a fused silica window was fitted to the DC-8 to enable acquisition of emission signatures in the near-UV region. The window has good and flat transmittance well below the atmospheric (ozone) cut-off at about 300 nm. The instrument was secured on top of a ball mount and pointed to the entering capsule by hand. A wide field of view video camera (a Watec device) with good performance at low light levels was co-aligned with the spectrometer to facilitate manual tracking which was achieved by displaying the video signal on a headset display with cross-hairs. The outlet of a tube delivering cold air was positioned near the window to prevent icing, and a curtain was placed over the mounted instruments during the observation event to prevent stray cabin light from entering the instruments.

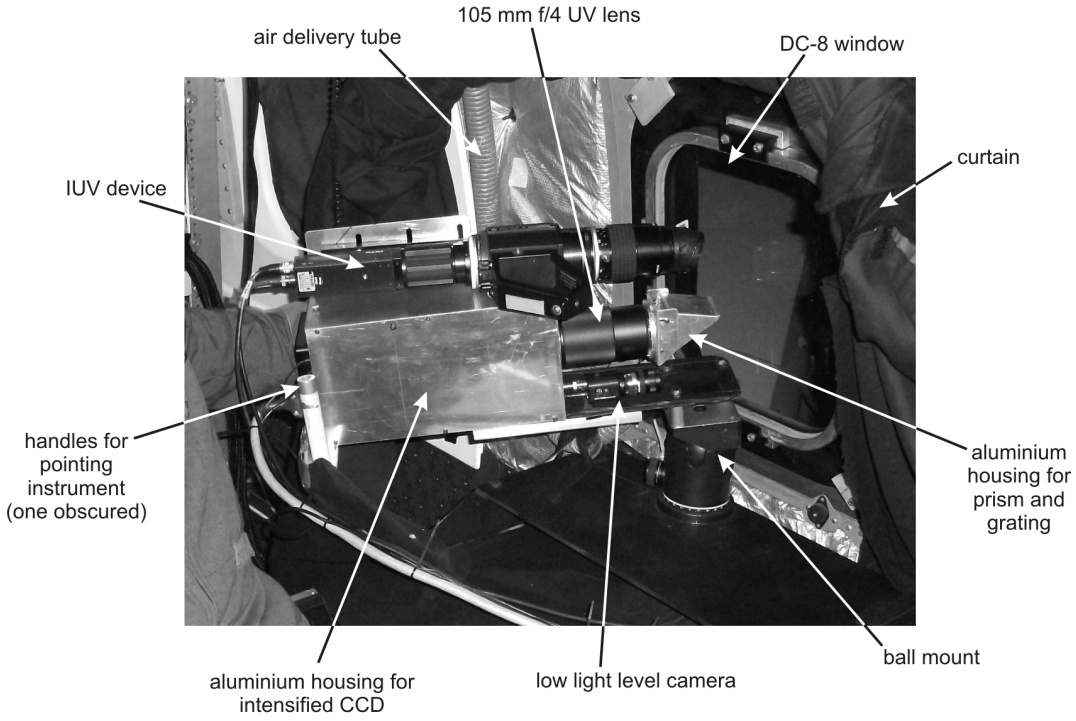

Figure 1. Annotated photograph showing the arrangement of the Australian Ultraviolet Spectrograph (AUS) mounted in the DC-8.

The design of the AUS instrument is illustrated in Fig. 2. The AUS instrument consisted of UV fused silica right angle prism (60 mm size, uncoated, Thorlabs: PS613) positioned ahead of a 1200 lines/mm fused silica transmission grating (50 × 50 mm, Thorlabs: GTU50-12). An offset of approximately 10 degrees was applied to the prism to achieve a centre wavelength of about 375 nm on the intensified CCD array. The right angle prism and

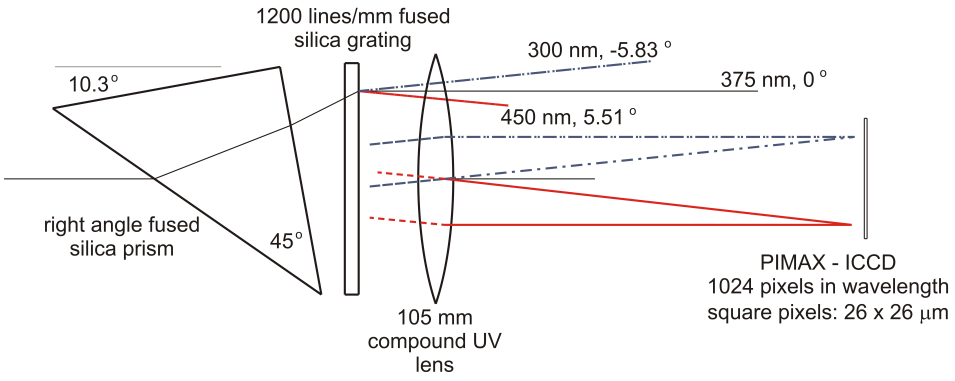

Figure 2. Optical arrangement of the Australian Ultraviolet Spectrograph (AUS).

diffraction grating were embedded in an aluminium housing with mating 52 mm filter mount. The 105 mm lens used in the AUS device was manufactured by CoastalOpt and had colour correction between 250 and 650 nm and an f/4.5 maximum aperture.

Imaging of the emissions was achieved using a Princeton Instruments intensified CCD camera (PI-MAX 1024B with a GenII intensifier) with 1024 × 256 pixels. The longer 1024 pixel rows were aligned in the vertical direction – the direction of the wavelength dispersion, providing a dispersion of 0.187 nm/pixel. The FWHM of Hg lines identified during wavelength calibrations was about 3 pixels, corresponding to a resolution of approximately 0.5 nm. The spectrometer field of view in the direction of the 256 pixels was approximately 3.6 degrees. Images were exposed for 100 ms and read-out and stored during a period of 269.536 ms to produce data at a rate of approximately one frame every 0.370 seconds. During the re-entry observation, the gain on the CCD intensifier was set to 200, and the lens aperture was set to its maximum.

III. Calibration

Calibrations of the AUS instrument were performed on the tarmac at the NASA Dryden Aircraft Operations Facility (DAOF) before and after the observation mission using NIST-traceable absolute radiance standard calibration lamps. Post-re-entry calibrations were also performed subsequently at the NASA Ames Research Center with an additional deuterium lamp for enhanced calibration accuracy at lower wavelengths.

Two standard integrating sphere lamps were used: a SphereOptics lamp fitted with a 500 $\pm$ 5 μm diameter aperture and a GigaHertz lamp (serial number BN-0102-02 SN14053aw, last calibrated April 9, 2010) fitted with a 809.1 $\pm$ 0.9 μm diameter aperture. These apertures were selected so that at the chosen calibration distance, both lamps produced peak irradiance similar to that anticipated for the capsule. However, because the anticipated near-UV

molecular band emissions from CN in the shock layer far exceeded the irradiance from the lamps at these wavelengths, it was necessary to calibrate the instrument using high exposure settings relative to those adopted for the re-entry observation. In all of the calibration work, Ocean Optics emission line halogen lamps containing mercury and argon (Hg/Ar) with small 1 mm apertures were placed at the same elevation adjacent to the standard lamps, in order to provide a wavelength scale for the calibration.

The standard spectral radiance values $L_{e,\lambda}$ (W/m^2-nm-sr) provided from the lamp calibrations were converted to spectral irradiance values $E_{e,\lambda}$ (W/m^2-nm) received at the instrument using the lamp aperture areas A_l, the solid angle of the flux received at the instrument Ω and the aperture area of the instrument, A_i according to

$$E_{e,\lambda} = \frac{L_{e,\lambda}\, A_l \Omega}{A_i}\,. \tag{1}$$

Because of the small solid angles used during calibration, to a very good approximation,

$$\Omega = \pi \left(\frac{r_i}{x}\right)^2 \tag{2}$$

where r_i is the radius of the instrument aperture and x is the distance from the source to the instrument aperture. Thus, the spectral irradiance received at the instrument location is independent of the instrument aperture as expected

$$E_{e,\lambda} = \frac{L_{e,\lambda}\, A_l}{x^2}\,. \tag{3}$$

Although the irradiance at the instrument during calibration is independent of the instrument aperture, the instrument sensitivity is dependent on the instrument aperture. For the present work the same aperture (f/4) was used during all calibrations and the observation flight. For the calibrations reported herein, the gain setting on the ICCD was 200, as it was for the observation flight.

For the calibrations performed on the tarmac at NASA Dryden Aircraft Operations Facility on 7 June 2010, the SphereOptics lamp was available to instruments towards the front of the DC-8 and was positioned close to boresight from the AUS instrument station. The distance from the lamp to the the outer skin of the aircraft at a point just above the window was measured with a laser range finder at 28.733 m. From the aircraft geometry, this location on the aircraft skin is estimated to be 80.3 mm closer to the AUS instrument than the outside surface of the fused silica window.[11] The window thickness was 31.75 mm and the distance from the inner window surface to the diaphragm of the 105 mm lens was 225 mm. Therefore, the overall distance from the lamp aperture to the instrument totals 28.906 m in this case.

For the 7 June 2010 results reported in Fig. 3, the pixel counts at each wavelength were

summed across 11 pixels in the spatial direction and the background counts were identified at each wavelength from the counts on pixels adjacent to the primary summation region. A total of 21 frames each with an exposure of 250 ms was recorded for this calibration so ADU results were averaged across the total number of frames and reduced in magnitude by a factor of 2.5 according to the ratio of exposure used during calibration to that used during the re-entry observation since the acquired counts are proportional to the exposure time. The instrument sensitivity figure expressed as ADU per W/m^2-nm was then obtained by dividing the summed counts (the ADU value) at each pixel location by the spectral irradiance $E_{e,\lambda}$ (Eq. 3) at the corresponding wavelength from the standard lamp. There is substantial scatter for this calibration despite the elevated exposure and the averaging over 21 frames, Fig. 3 . At 460 nm, the mean sensitivity deduced from the 7 June 2010 calibrations was 1.170×10^{13} ADU per W/m^2-nm with the standard deviation over 32 pixels centered at this wavelength being 0.089×10^{13} ADU per W/m^2-nm.

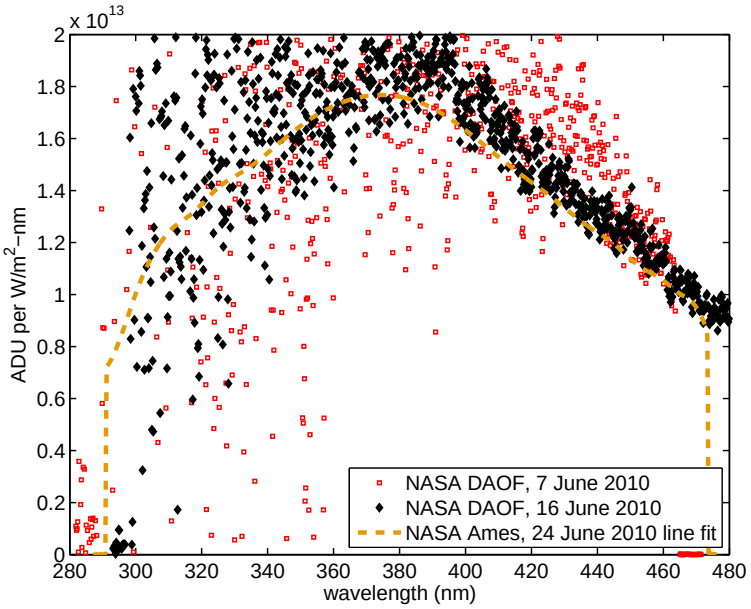

Figure 3. Instrument sensitivity results from pre- and post-re-entry calibrations on the tarmac at NASA Dryden Aircraft Operations Facility referenced to the settings used during the re-entry observation.

A similar approach was adopted for the 16 June 2010 tarmac calibrations except that in an effort to improve the signal-to-noise ratio, 5 frames with 20 accumulations at an exposure of 200 ms were recorded. In this case, the distance from the lamp to the instrument was 27.666 m, and the lamp used for this calibration was the GigaHertz device. A substantial improvement in the signal to noise ratio was achieved – the standard deviation of the signal over 32 pixels centered at 460 nm was 0.057×10^{13} ADU per W/m^2-nm compared with a figure of 0.089×10^{13} ADU per W/m^2-nm achieved in the pre-flight calibration. The mean sensitivity at this wavelength was 1.096×10^{13} ADU per W/m^2-nm in the post-flight tarmac calibration and this figure is approximately 6 % lower than the value identified from pre-flight

calibrations with the SphereOptics lamp. The post-flight calibrations with the GigaHertz lamp are considered more reliable because of the improvements in the signal-to-noise ratio that were achieved through instrument settings adopted for the post-flight calibration, and because post-flight calibrations with the SphereOptics lamp consistently indicate a reduction in lamp output by around 50 % relative to pre-flight lamp output[11] and this reduces confidence in the absolute calibration of the SphereOptics lamp.

Further improvements in the calibration methods were achieved during additional post-flight calibrations performed at the NASA Ames Research Center on 24 June 2010. For this work, the signal-to-noise ratio of the calibration was increased for wavelengths lower than 400 nm through the use of a deuterium lamp with a defined spectral radiance which was co-aligned with the GigaHertz integrating sphere. These two lamps in combination provided reference irradiance standards down to the lowest wavelength limit of the AUS instrument. An Hg/Ar lamp was also co-aligned with the standard lamps in order to provide the wavelength reference. For this work, one of the fused silica windows as used on DC-8 was taken to the laboratory, and the lamps were positioned 25.730 m from the window. The AUS instrument was positioned on the other side of the window, directly facing the calibration lamps. The total distance from the lamps to the diaphragm of the 105 mm lens was 25.958 m in this case. For the calibrations with the integrating sphere, 20 frames were taken, each with 75 accumulations at an exposure of 100 ms on the ICCD. For the deuterium lamp, 20 frames were taken with one accumulation at an exposure of 60 ms. Results from these calibrations are presented in Fig. 4, again referenced to a single accumulation at an exposure of 100 ms as was used for the re-entry observation event.

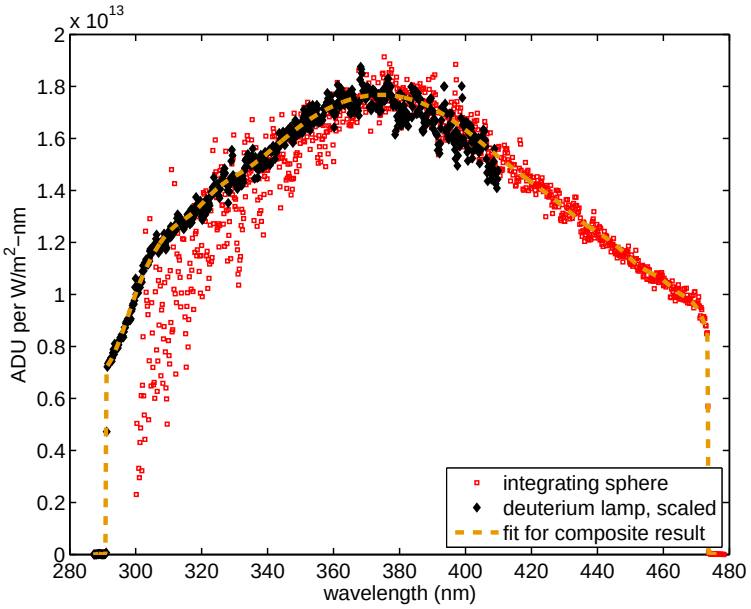

Figure 4. Instrument sensitivity results from the calibrations performed at NASA Ames Research Center referenced to the settings used during the re-entry observation.

Although an absolute radiance calibration was provided with the deuterium lamp, the uncertainties in the actual discharge area of this lamp make it necessary to rely on the integrating sphere for an absolute fix on the irradiance provided to the AUS instrument. Therefore the instrument sensitivity results from the deuterium lamp were scaled to match the results from the integrating sphere at a wavelength of 370 nm, corresponding to the peak sensitivity of the instrument. The instrument sensitivity deduced from the scaled deuterium lamp calibrations closely follows that derived from the GigaHertz lamp at wavelengths either side of the selected cross-over wavelength (370 nm) and this demonstrates the reliability of the deuterium lamp scaling method. Over 32 pixels centered at 460 nm, the mean of the instrument sensitivity figure in this case is 1.048×10^{13} ADU per W/m^2-nm with a standard deviation of 0.023×10^{13} ADU per W/m^2-nm. Given the calibrations performed at NASA Ames yielded considerably better signal-to-noise and seemingly reliable results down to the lowest wavelength detection limits of the AUS instrument, these calibration results are adopted for the analysis of the re-entry observation data. The cubic spline curve fitted to the calibration data shown as the broken line in Fig. 4 is used to facilitate data analysis.

IV. Results

IV.A. Observation Overview

First light from the spacecraft was recorded on the ICCD at 13:51:54.0 UTC with the capsule first appearing distinct from the main bus at 13:52:00.3 UTC. The proximity of the capsule and spacecraft bus on the ICCD image for times before 13:52:12.1 UTC introduced some uncertainty in identification of the capsule spectra and some localized interference from the main bus spectra also occurred. Bright emissions from the disintegrating main bus caused localised saturation on the ICCD and serious distortion of the counts recorded in imaging of the capsule spectra for times between 13:52:12.1 and 13:52:17.2 UTC, rendering the data in the capsule region unusable during this time. High counts in the main bus region recorded on the ICCD continued to distort some of the results in the capsule region from 13:52:17.6 to 13:52:21.0 UTC but from 13:52:21.3 UTC, counts from the disintegrating main bus were no longer problematic. From 13:52:28.0 UTC, disintegrating bus fragments were no longer recorded on the ICCD and by 13:52:36.1 UTC, the counts from the capsule region were comparable to the background noise recorded on the ICCD.

IV.B. Data Analysis

Sample results from a frame recorded at 13:52:05.40 UTC are presented in Fig. 5. In this figure the primary feature of the ICCD image is the main bus, but the capsule region can

be seen just below the main bus region. For the orientation of ICCD image of Fig. 5, the direction of increasing wavelength is towards the right of the page, and the direction of capsule travel is towards the bottom of the page. To define the capsule region, a strip of around 8 or more pixels (in the spatial direction) was manually identified for each frame, and the counts within this strip were summed in the spatial direction. The width of the pixel strip identified for each frame actually varied depending on motion blur arising from imprecise tracking of the capsule during the period of exposure of the ICCD frame (100 ms). When motion blur resulted in smearing in both the spatial and the wavelength directions, it was generally possible to track a spectral feature across adjacent pixels rows, and summation of the capsule counts at each wavelength was then performed along this oblique direction.

To identify the appropriate background level for subtraction from the capsule region results, the counts along two rows of pixels, one immediately above and the other immediately below the capsule region (in the orientation of the ICCD image in Fig. 5) were averaged across 3 pixels in the wavelength direction. The background counts across the capsule region was then taken to be a linear variation in the spatial direction between the counts identified from the strip of pixels above and below the capsule region. A spectral feature within the net counts from the capsule region and the calibrated dispersion of the instrument (0.187 nm/pixel) allowed the assignment of wavelengths to each pixel. The net counts from the capsule region at each wavelength was then divided by the sensitivity figure of the instrument at each corresponding wavelength (Section III) to determine the spectral irradiance received at the DC-8 location.

To assess the likely precision with which the background counts can be estimated using the linear variation described above, two approaches were taken. First, in the case of the early frames, prior to rapid disintegration of the bus region and while the imaged bus region appeared largely symmetric in the spatial direction, a reference capsule region was identified as illustrated in Fig. 5. The reference capsule region is the same size as the actual capsule region and is located the same number of pixels behind the bus as the actual capsule region is located ahead of the bus. The background subtraction method that was adopted for the actual capsule region was applied to the reference capsule region so that the total counts actually recorded in the reference capsule region could be compared with the total counts estimated according to the linear background subtraction method. It was found that linear background approximation generally overestimated the background counts. The magnitude of the error varied with wavelength, being largest at around 385 nm. The magnitude of the background subtraction error was largely independent of the net counts in the imaged capsule region for each frame. For wavelengths around 355 nm, the background subtraction error for times between 13:52:1.7 and 13:52:12.1 UTC was around 6 % of the irradiance received at around 13:52:20 UTC. For wavelengths around 385 nm, the corresponding error was about

10 %.

The second approach for estimating the precision of the background subtraction method was applied in the case of frames after 13:52:21.3 UTC, and a representative ICCD image and corresponding spectral irradiance result for such times is presented in Fig. 6. The assessment of the background subtraction method in these cases involved the identification of a reference capsule region immediately ahead of the actual capsule on the ICCD image. The same assessment method discussed in the previous paragraph was applied in these cases and indicated that in reference capsule region, the linear approximation generally overestimated the background. The magnitude of the error in this case varied with the local magnitude of the imaged capsule emissions, with two times the standard deviation of the error being around 8 % of the capsule spectral irradiance. Given the uncertainty in the variation of the effective background in the capsule region relative to the region ahead of the capsule, it is appropriate to consider the uncertainty as ±8 % of the capsule spectral irradiance for frames after 13:52:21.3 UTC.

Results in Fig. 6(b) show emissions from a variety of molecular and atomic species superimposed on the continuum emissions from the capsule surface. The principal species contributing to observed molecular radiation are N_2^+ and CN. Carbon is a major element of Hayabusa's carbon phenolic ablator thermal protection system so CN is expected to be generated primarily through the combination of dissociated nitrogen in the high temperature shock layer air and ablation products from the heat shield. Calcium lines (Ca and Ca^+) are also apparent and on close inspection, aluminium lines can also be observed between the two Ca^+ lines.

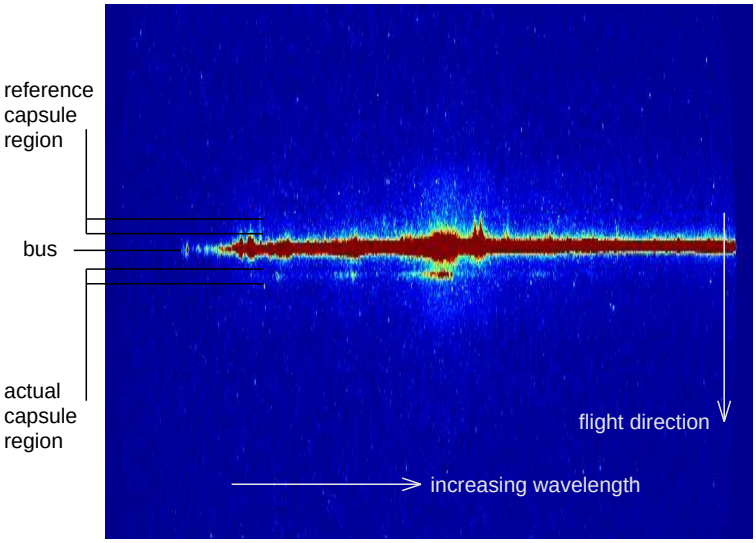

Figure 5. ICCD image acquired at 13:52:05.40 (UTC) (presented in false colour and an expanded spatial scale) illustrating the location of the Hayabusa capsule and the spacecraft bus.

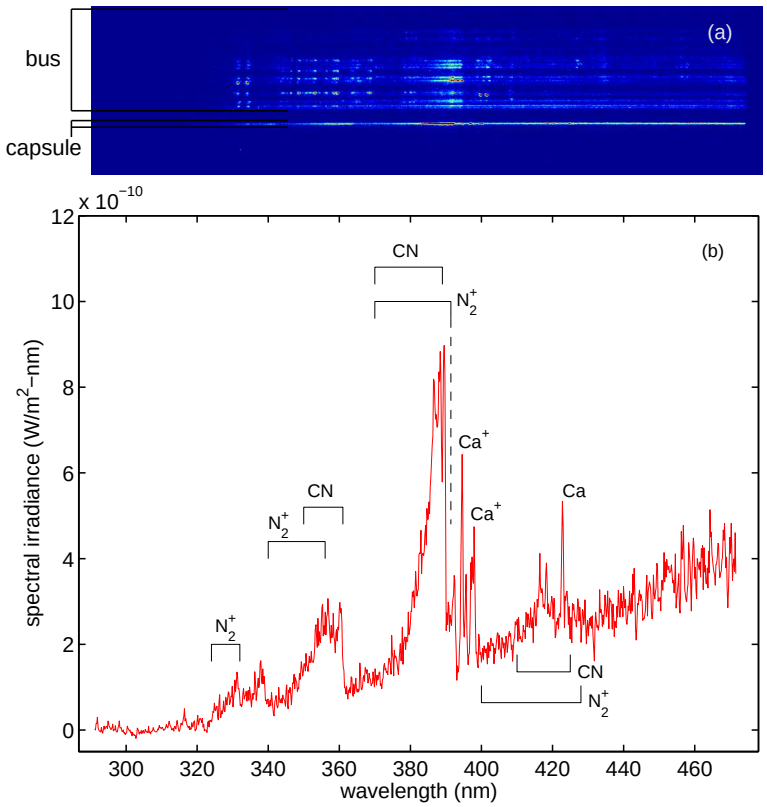

Figure 6. Results acquired at 13:52:22.40 (UTC). Part (a): ICCD image (false colour) illustrating the location of the capsule and the disintegrating spacecraft bus. Part (b): spectral irradiance received at the DC-8.

IV.C. Irradiance referenced to 100 km, front view, no extinction

Results from the analysis of the recorded data were presented in terms of the spectral irradiance received at the DC-8 in an earlier publication.[12] Figures 7, 8, 9, 10 and 11 give the spectral irradiance results scaled in the manner described below so as to present the irradiance hypothetically received from the capsule in the absence of atmospheric extinction at a distance of 100 km with the capsule viewed head-on at every point in time. Results in Figs. 7 to 11 have been averaged over 3 frames. In cases where emissions from the disintegrating bus have contaminated the capsule results in distinct wavelength bands only (between times 6.5 and 18.7 s), results within the corrupted wavelengths have been removed. Results at times 19.1, 20.6 and 21.0 seconds (corresponding to frames 96, 100 and 101) have been presented in a light shade because these frames were subject to either uncorrectable motion blur or background subtraction errors which were not accommodated with the standard approach described in Section IV.B. Reliable results for times between 13:52:12.1 and 13:52:17.6 UTC were not obtained because during this period, extremely bright emissions from the disintegrating bus corrupted the imaging of spectra from the capsule.

To achieve the scaling of the irradiance results presented in Figs. 7 to 11, Modtran simulations of the spectral transmittance through the atmospheric path length between the

capsule and DC-8 location were performed for the capsule at a number of altitudes between 100 and 40 km, based on the predicted locations of both the capsule and DC-8. For each frame acquired on the ICCD, the Modtran results were interpolated to determine the instantaneous transmittance which applied at that point in time and the DC-8 received irradiance results were then scaled by the inverse of the transmittance value at each wavelength. The presence of ozone virtually extinguishes the atmospheric transmission for wavelengths approaching 300 nm so the irradiance results in Figs. 7 to 11 have only been presented for wavelengths larger than about 320 nm because attempting to scale the irradiance received at the DC-8 using a quantity which tends to infinity greatly amplifies the noise at lower wavelengths.

The DC-8 was positioned such that when the capsule was in the field of view, the full front surface of the capsule would be seen, albeit at an oblique angle. Therefore, to transform the received irradiance at the DC-8 to the reference conditions of 100 km and frontal view, the DC-8 irradiance results were scaled by the ratio

$$\left(\frac{100}{d_{obs}}\right)^2 \frac{\pi\, r_{cap}^2}{A_{obs}} \tag{4}$$

where d_{obs} is the instantaneous observed distance (km) between the capsule and the DC-8, r_{cap} is the actual capsule radius (0.2 m) and A_{obs} is instantaneous area of the capsule face observed from the DC-8. Values for d_{obs} and A_{obs} were deduced from pre-flight simulations of the capsule re-entry path and location relative to the aircraft and have been tabulated in a separate paper.[11]

The growth and decay of the CN and N_2^+ bandhead features can be discerned throughout Fig. 7 to 11, and from 13:52:17.6 UTC, the low-wavelength tail of the gray body radiation emitted from the heat shield is identified as the feature underlying the plasma emissions. The Ca line at 422.79 nm can be identified from 13:52:17.6 UTC and this is the spectral feature which was used to specify the wavelength scale at these times.

Figures 7 to 11 include results from the HDVS1 instrument[11] for wavelengths down to almost 400 nm, demonstrating consistency between the AUS results and the HDVS1 results in the wavelength overlap region, although the magnitude of HDVS1 spectral irradiance generally appears to increase with wavelength at a higher rate. Also presented in these figures are gray-body Planck curves fitted to the AUS results by matching the spectral irradiance value at 457.5 nm (taken as the average of values between 455 and 460 nm) and assuming an emissivity of 0.9. The values of apparent capsule temperature deduced in this manner are presented in Section IV.D and are consistent with temperature values deduced with other instruments. These Planck curves also appear to provide a reasonable baseline level for assessment of emissions from the shock and ablation layers.

IV.D. Temporal development of radiation

Figure 12 illustrates the development of irradiance within two wavelengths bands which cover the region of CN and N_2^+ bandheads (B-X) $\Delta\nu = 0$ (365 to 392 nm) and $\Delta\nu = -1$ (345 to 365 nm). These irradiance results were obtained by integrating the spectral irradiance results in Figs. 7 to 11 over the respective wavelength regions. In the case of the Planck results shown in Fig. 12, these were obtained from a similar integration, this time of the Planck curves also shown in Figs. 7 to 11, with values between the times of 11 and 18 seconds derived from the HDVS1 data.[11] The error bars on the data Fig. 12 represent uncertainties associated with the background subtraction methods as discussed in Section IV.B.

In the case of the data up to 11 seconds, the error bars are unidirectional and are unique to each frame (data point), being derived from the background subtraction assessment process for each frame which was introduced in Section IV.B. For the data prior to 11 seconds, most of the error bars reach in the positive direction, indicating that the magnitude of the background is likely underestimated in these cases. In the case of the data after 18 seconds, the presented error bars are bidirectional and are indicative of the $\pm 2\sigma$ uncertainties associated with the background subtraction method in the absence of distortion effects from the spacecraft bus.

Radiation from the $\Delta\nu = 0$ bandhead first peaks at around 7 seconds, and at this time the radiation from the $\Delta\nu = -1$ bandhead appears to plateau. Although emissions from the main bus contaminated the capsule radiation data in the period from 11 seconds to 18 seconds, radiation from both bandheads must increase some time during this period because irradiance peaks with a magnitude approximately double that of the first peak/plateau are observed for both bandheads at around 20 seconds.

Apparent capsule temperature results presented in Fig. 13 were identified from Planck irradiance values which were fitted to the AUS data at a wavelength of 457.5 nm (taking a mean value of the irradiance from 455 to 460 nm), and to the HDVS1 data[11] at a wavelength of 462.5 nm (taking a mean value of the irradiance from 460 to 465 nm). In each case, the data points in Fig. 13 represent the values obtained with an assumed emissivity of 0.9, and the error bars represent the higher and lower temperature limits which would be obtained for emissivities of 0.8 and 1.0 respectively. Capsule temperature results differing from those of Fig. 13 by up to 200 K can be obtained from other spectral irradiance data,[11] depending on the wavelength region and the methodology used for fitting the Planck curve. Nevertheless, the results in Fig. 13 demonstrate the consistency of AUS and HDVS1 results in the vicinity of 460 nm.

V. Conclusion

The Australian Ultraviolet Spectrograph, a slit-less device, was developed for remote observation of the near-UV emissions from the re-entry of JAXA's Hayabusa which occurred above Australia late in the evening of 13 June 2010. Spectra within the wavelength range 300 – 470 nm were successfully acquired from NASA's DC-8 platform which was positioned just outside the designated re-entry corridor during the event. The capsule emissions were distinguished from the spacecraft bus emissions from 13:52:1.7 UTC but for times between 13:52:12.1 and 13:52:17.6 UTC, very bright emissions from the disintegrating spacecraft bus corrupted the imaging of the capsule emissions.

Calibrations of the instrument before and after the event has enabled deduction of absolute spectral irradiance from the capsule and surrounding shock layer. Results demonstrate the temporal development of emissions from species associated with the shock layer and heat shield material including N_2^+, CN, Al, Ca, and Ca^+. In particular, the strong emissions within the CN and N_2^+ manifolds $\Delta\nu = 0$, $\Delta\nu = -1$, and $\Delta\nu = +1$ are clearly identified in the spectra. The low-wavelength tail of gray-body emissions from the heat shield is also observed with the AUS instrument from 13:52:17.6 UTC.

The magnitude of spectral irradiance obtained with the instrument compares very favourably with those obtained from an independently calibrated and operated instrument[11] for overlapping portions of spectra from each instrument: the region from 410 to 470 nm. The agreement between these two independent instruments is reflected in the deduction of apparent capsule temperatures: both instruments give a peak in the apparent temperature of approximately 3050 K at around 13:52:23 UTC based on irradiance measurements in the vicinity of 460 nm and an assumed heat shield emissivity of 0.9.

Uncertainties in the absolute irradiance values reported for the instrument arise primarily due to background subtraction. For times between 13:52:1.7 and 13:52:12.1 UTC, the background subtraction uncertainty varies with wavelength and amounts to between 6 and 10 % of the irradiance received at 13:52:20 UTC. For times after 13:52:17.7 UTC, the uncertainty scales approximately with the instantaneous irradiance, a representative $\pm 2\sigma$ value being ± 8 %.

The data presented in this paper are expected to be used in the on-going validation and development of super-orbital computational tools in the near future. Expansion tunnel simulation of the Hayabusa re-entry with duplication of the super-orbital flow enthalpies and correctly scaled density are also being planned for the X2 and X3 facilities in efforts to explore the fidelity of ground-based test facility simulations of such conditions.

Acknowledgments

Support through the The Australian Research Council Discovery program is acknowledged. The University of Southern Queensland and The University of Queensland provided support which enabled the travel and the development of the instrument for the Hayabusa observation mission. NASA is thanked for the invitation to participate in the airborne observation mission, Drs Stefan Loehle and Michael Winter are thanked for discussions on instrument operation and settings, and for assistance with instrument calibrations, and Dr Tetsuya Yamada of JAXA is thanked for facilitating the appointment of Hayabusa observers to the Hayabusa Joint Science Team. The observing campaign was funded by the NASA In-Space Propulsion Technology Program. The SETI Institute was supported under cooperative agreement NNX10AH17A.

References

[1]Morgan, R. G., McIntyre, T. J., Buttsworth, D. R., Jacobs, P. A., Potter, D. F., Brandis, A. M., Gollan, R. J., Jacobs, C. M., Capra, B. R., McGilvray, M., and Eichmann, T. N., "Impulse facilities for the simulation of hypersonic radiating flows." *38th Fluid Dynamics Conference and Exhibit*, AIAA Paper 2008-4270, American Institute of Astronautics and Aeronautics, June 2008.

[2]Buttsworth, D. R., D'Souza, M., Potter, D., Eichmann, T., Mudford, N., McGilvray, M., McIntyre, T. J., Jacobs, P., and Morgan, R., "Expansion Tunnel Radiation Experiments to Support Hayabusa Reentry Observations," *48th AIAA Aerospace Sciences Meeting*, AIAA Paper 2010-634, Orlando, Florida, 4 – 7 January 2010.

[3]Jenniskens, P., "Observations of the Stardust Sample Return Capsule Entry with a slitless Echelle spectrograph," *Journal of Spacecraft and Rockets*, Vol. 47, No. 5, 2010, pp. 718–735.

[4]Boyd, I. D., Trumble, K. A., and Wright, M. J., "Modeling of Stardust Entry at High Altitude, Part 1: Flowfield Analysis," *Journal of Spacecraft and Rockets*, Vol. 47, 2010, pp. 708–717.

[5]Boyd, I. D. and Jenniskens, P., "Modeling of Stardust Entry at High Altitude, Part 2: Radiation Analysis," *Journal of Spacecraft and Rockets*, Vol. 47, 2010, pp. 901–909.

[6]Eichmann, T., Khan, R., McIntyre, T., Jacobs, C., Porat, H., Buttsworth, D., and Upcroft, B., "Radiometric temperature analysis of the Hayabusa spacecraft re-entry," *28th International Symposium on Shock Waves*, Manchester, UK, 17 – 22 July 2011.

[7]Winter, M. W. and trumble, K. A., "Near-Ultraviolet Emission Spectroscopy During an Airborne Observation of the Stardust Reentry," *Journal of Spacecraft and Rockets*, Vol. 48, No. 1, 2011, pp. 59–71.

[8]Rairden, R. L. and Jenniskens, P., "Near-Ultraviolet Spectroscopy of the Stardust Sample Return Capsule Reentry," *Journal of Spacecraft and Rockets*, Vol. 47, No. 5, 2010, pp. 753–756.

[9]Jenniskens, P., Koop, M., and Albers, J., "Intensified Low-Resolution Optical Spectroscopy of the Stardust Sample Return Capsule Entry," *Journal of Spacecraft and Rockets*, Vol. 47, No. 6, 2010, pp. 895–900.

[10]Jenniskens, P., Wilson, M. A., Winter, M., and Laux, C. O., "Resolved CN Band Profile of Stardust Capsule Radiation at Peak Heating," *Journal of Spacecraft and Rockets*, Vol. 47, No. 6, 2010, pp. 873–877.

[11]Jenniskens, P., Kozubal, M. J., Dantowitz, R. F., Winter, M. W., and Loehle, S., "Time-resolved absolute irradiance of the Hayabusa sample return capsule reentry," *50th Aerospace Sciences Meeting*, Nashville, Tennessee, 9–12 January 2012.

[12]Buttsworth, D., Morgan, R., and Jenniskens, P., "Near Ultraviolet Emission Spectroscopy of the Hayabusa Re-entry," *50th AIAA Aerospace Sciences Meeting*, AIAA Paper 2012-1297, Nashville, Tennessee, 9 – 12 January 2012.

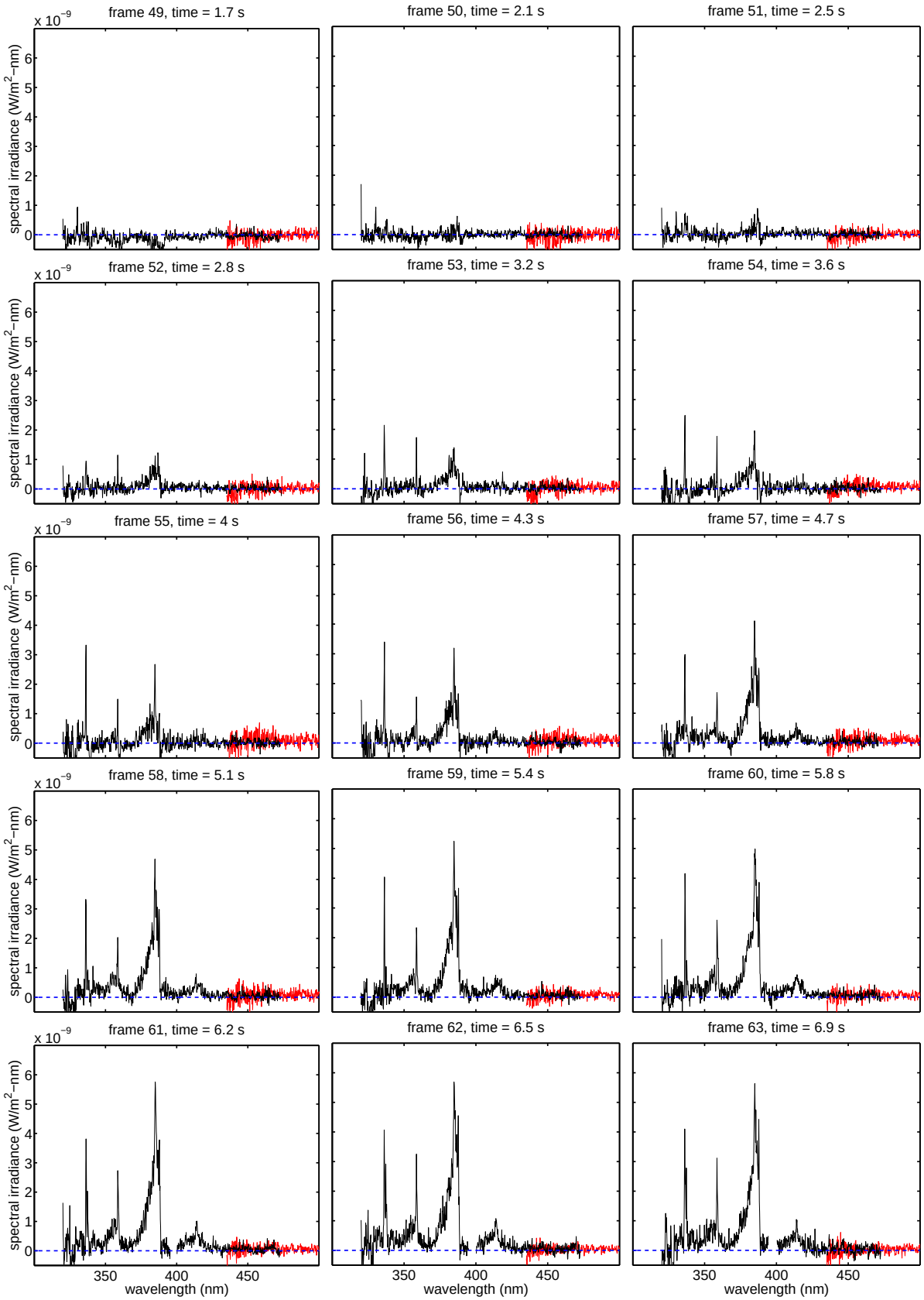

Figure 7. Spectral irradiance from the capsule for times between 1.7 s and 6.9 s relative to 13:52:00 UTC. Black line: AUS result; line with lighter shade (for $\lambda > 400$ nm): HDVS1 result; broken line: Planck curve fit.

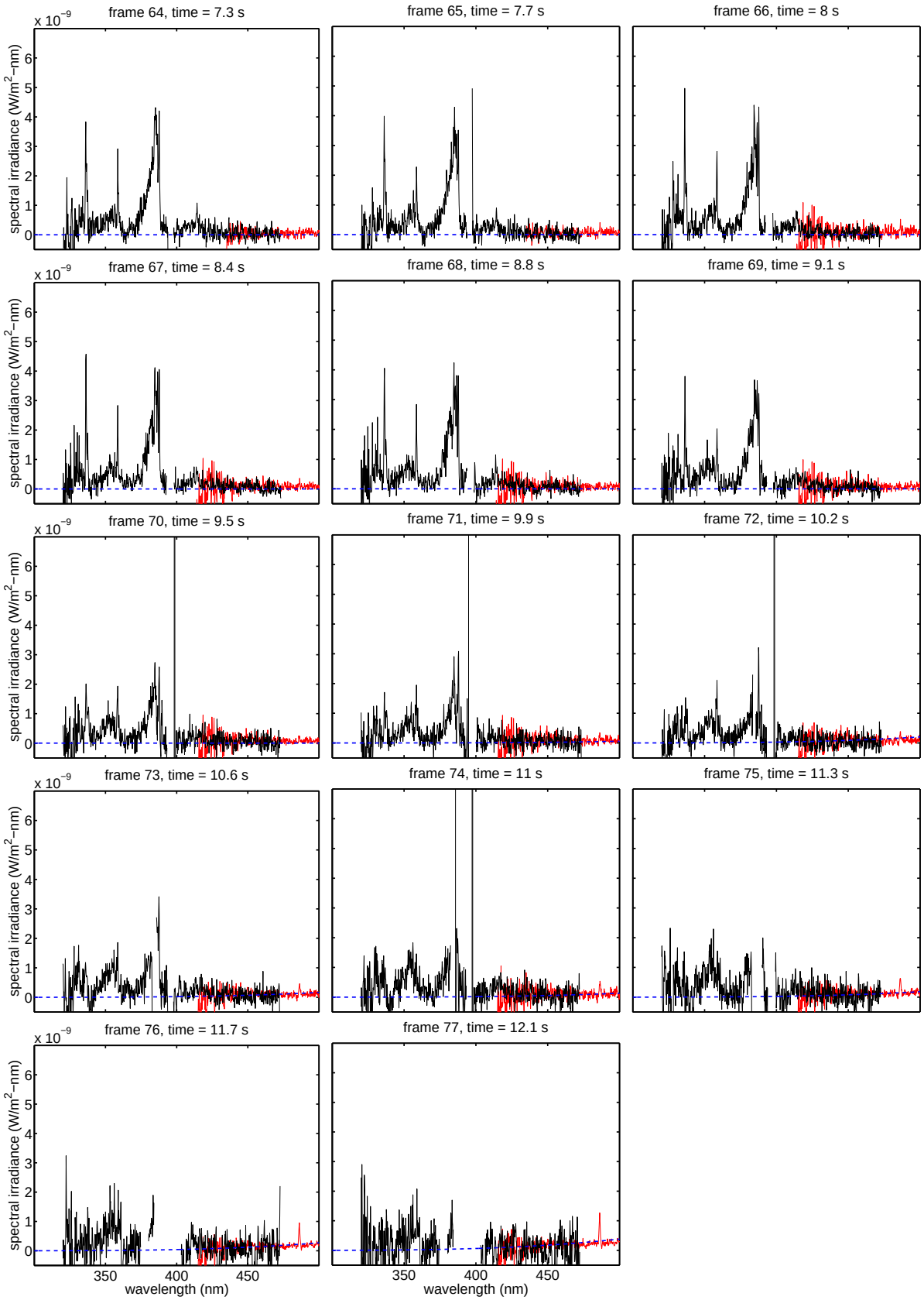

Figure 8. Spectral irradiance from the capsule for times between 7.3 s and 12.1 s relative to 13:52:00 UTC. Black line: AUS result; line with lighter shade (for $\lambda > 400$ nm): HDVS1 result; broken line: Planck curve fit.

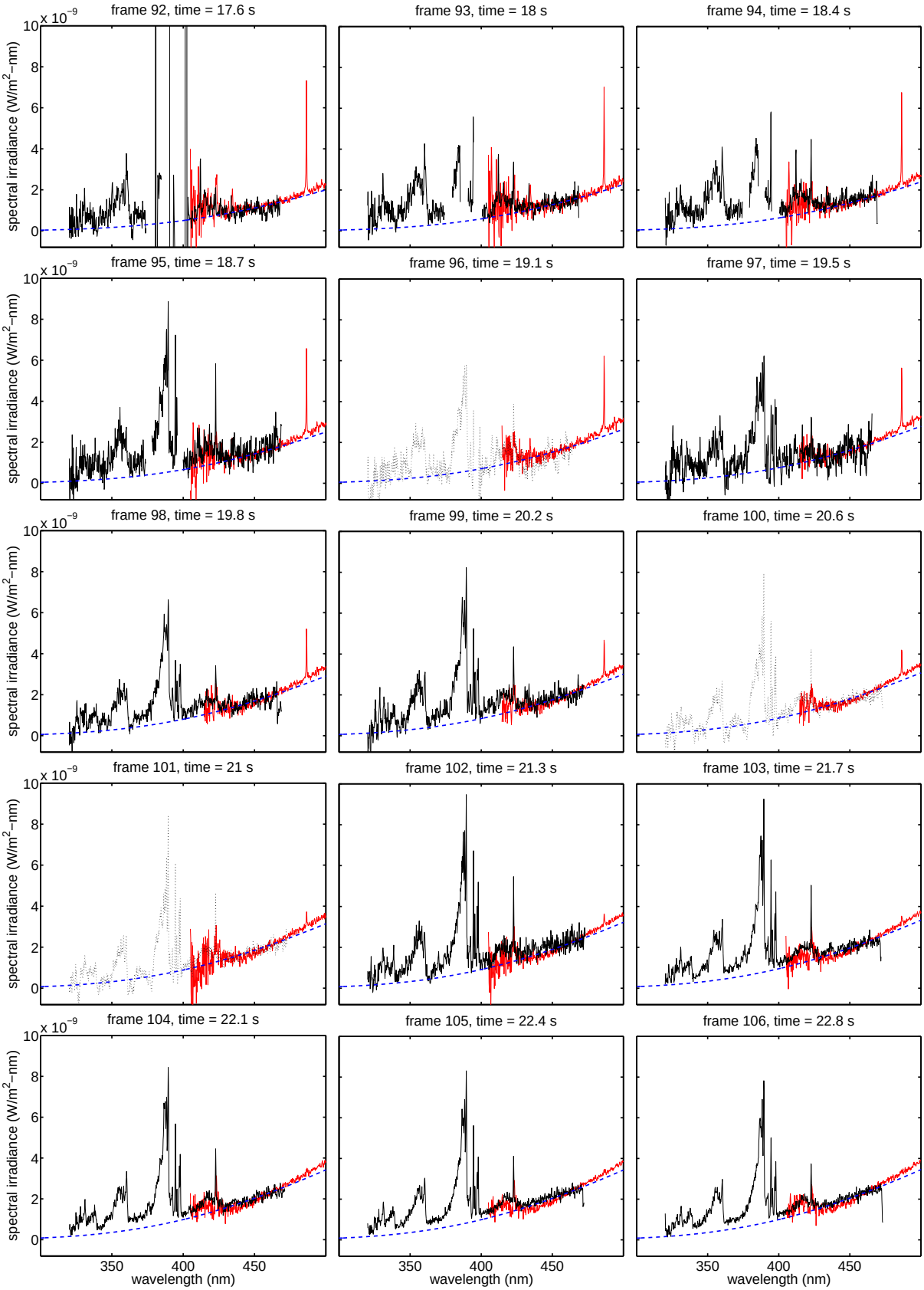

Figure 9. Spectral irradiance from the capsule for times between 17.6 s and 22.8 s relative to 13:52:00 UTC. Black line: AUS result; line with lighter shade (for $\lambda > 400$ nm): HDVS1 result; broken line: Planck curve fit.

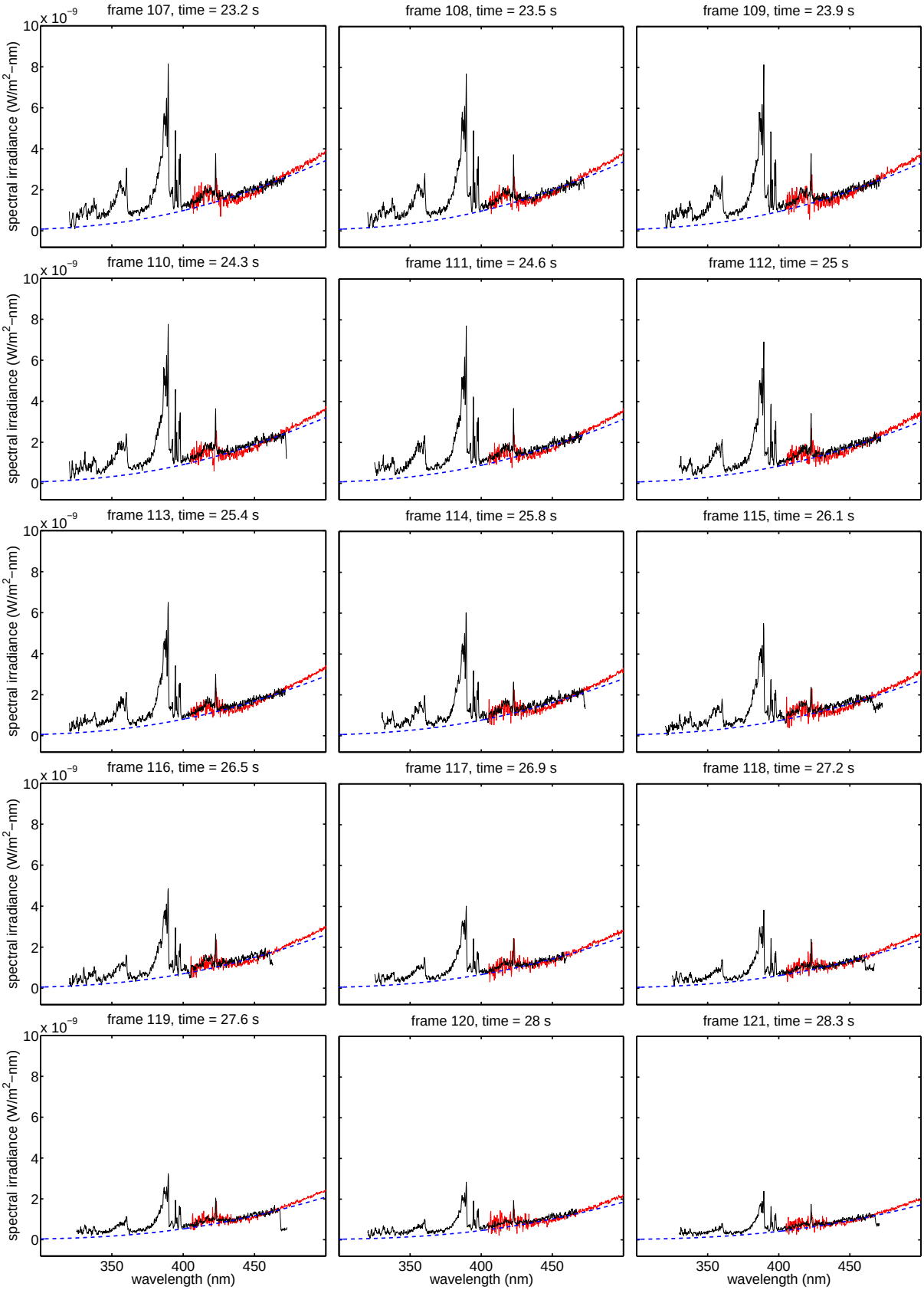

Figure 10. Spectral irradiance from the capsule for times between 23.2 s and 28.3 s relative to 13:52:00 UTC. Black line: AUS result; line with lighter shade (for $\lambda > 400$ nm): HDVS1 result; broken line: Planck curve fit.

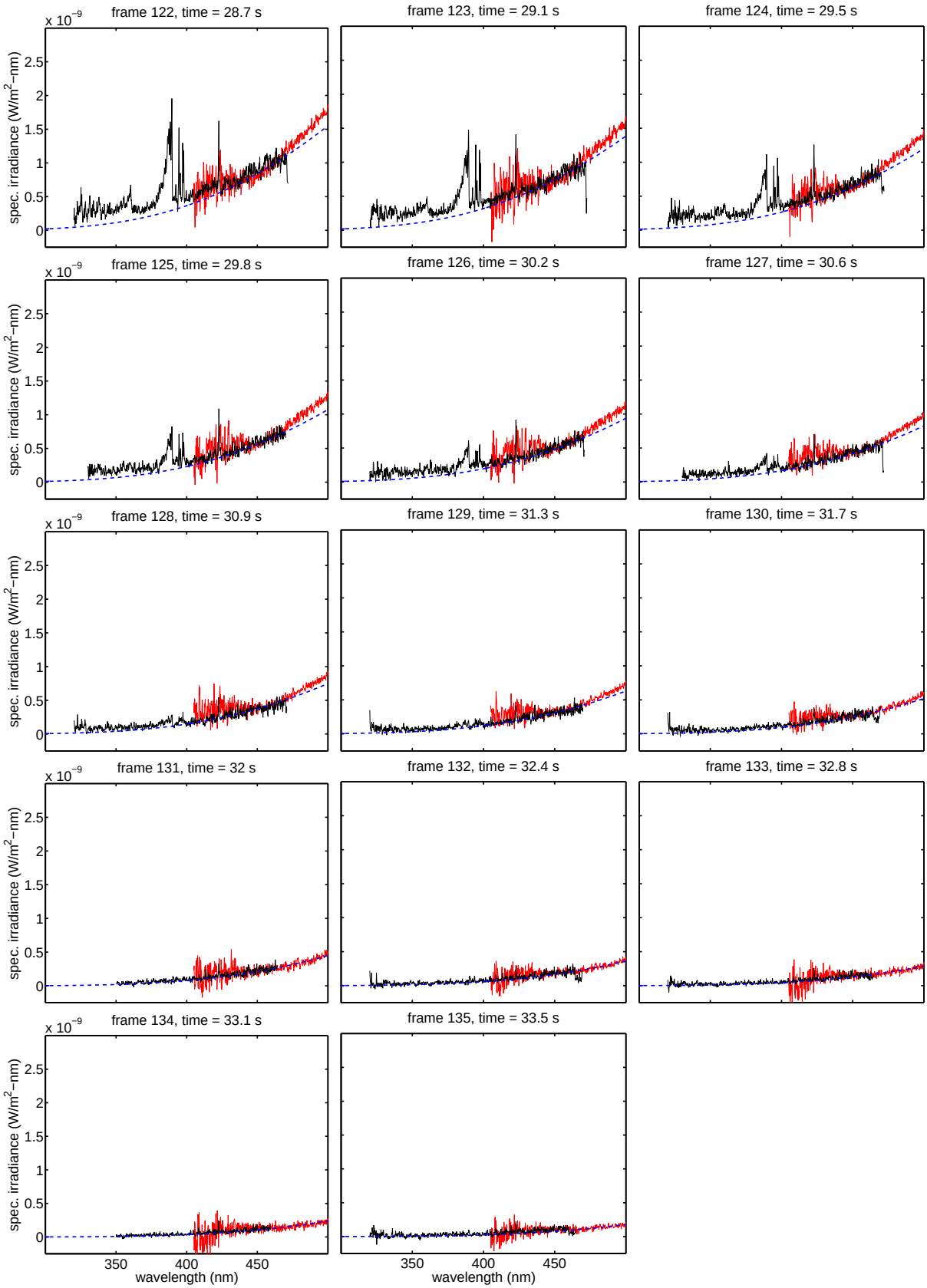

Figure 11. Spectral irradiance from the capsule for times between 28.7 s and 33.5 s relative to 13:52:00 UTC. Black line: AUS result; line with lighter shade (for $\lambda > 400$ nm): HDVS1 result; broken line: Planck curve fit.

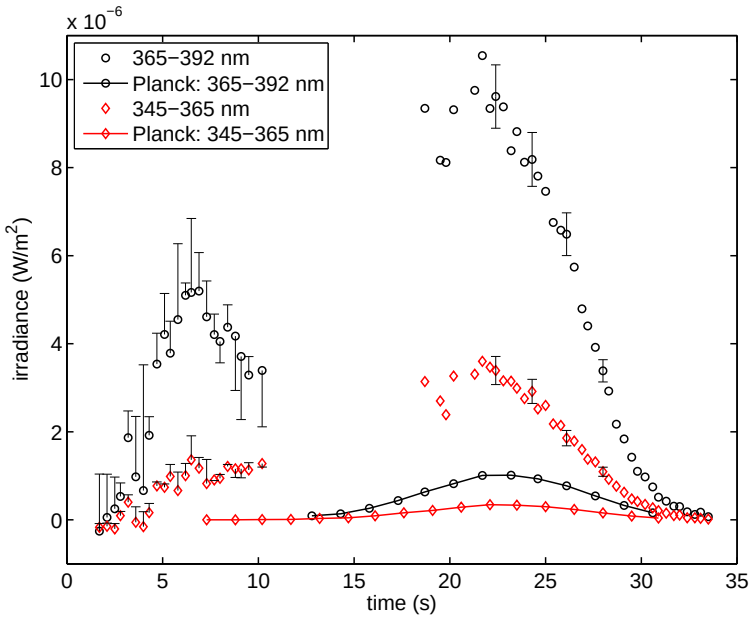

Figure 12. Development of irradiance as a function of time for two wavelength bands covering the combined emisssions from the CN and N_2^+ bandheads: (B-X) $\Delta\nu = 0$ and $\Delta\nu = -1$.

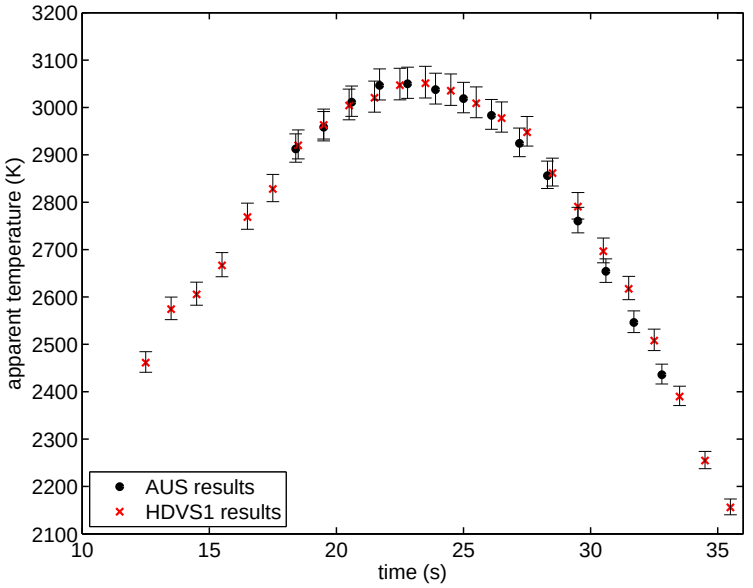

Figure 13. Apparent capsule temperature as a function of time for an assumed emissivity of 0.9 with the limits of the error bars indicating the temperatures corresponding to emissivity values of 0.8 and 1.0.